Rev. Cub. Física vol. 26, No. 1 (2009) p 42-46
ISSN: 0253-9268. Original paper

Revista Cubana de Física
Calle I No. 302 e/ 15 y 17
Vedado, La Habana. CP 10400
www.fisica.uh.cu/biblioteca/revcubfi/index.htm

TeO_2-doped ZnO micro and nanostructures grown by the vapour–solid technique

A. Iribarren[a,b,†], P. Fernández[b] y J. Piqueras[b]

a) Instituto de Ciencia y Tecnología de Materiales, Universidad de La Habana, Zapata y G, Vedado, Ciudad de La Habana 10400, Cuba; augusto@fisica.uh.cu
b) Departamento de Física de Materiales, Facultad de Ciencias Físicas, Universidad Complutense de Madrid, 28040, Madrid, Spain
† Autor para la correspodendia

Received 8/04/2009. Approved in final version 18/06/09

Sumario. Se presenta la obtención de micro y nanoestructuras a partir de polvos de ZnO impurificados con TeO_2 por un proceso vapor-sólido. Se realizaron mediciones topológicas y catodoluminiscentes (CL) de las muestras y estructuras. Se encontró que las estructuras están formadas por una mezcla de dominios de ZnO y $ZnTe_xO_{1-x}$ y que los átomos de Te en los sitios de las vacancias de oxígeno juegan un rol pasivante que puede eliminar los defectos. Las mediciones de CL y el mapeo permitieron describir las características locales de las muestras y de estructuras representativas.

Abstract. An approach for the obtaining of nano and microstructures from TeO_2-doped ZnO powder by vapour-solid process technique is presented. Topological and cathodoluminescence (CL) measurements of the samples and structures were carried out. It was found that the structures are formed by a mixture of ZnO and $ZnTe_xO_{1-x}$ domains, and that in Te atoms in oxygen vacancy sites play a passivating role that can eliminate the defects. The local features of samples and representative structures were study by means of CL measurements and mapping.

Keywords: Cathodoluminescence, 78.60.Hk, fabrication of nanostructures 81.07.-b

1 Introduction

Low dimensional semiconductor structures constitute one of the subjects of increasing interest since they have potential application in several technological fields as for nanoelectronic systems and photovoltaics. Besides their attractive shapes, optical and compositional behaviours along the structures constitute relevant features to be studied.

ZnO is typically unintentionally doped *n* type wide-gap semiconductor due to the lack of stoichiometry resulting mainly from oxygen vacancies. Its band gap energy has been reported to be between 3.2 and 3.37 eV[1-3]. Oxygen vacancies (V_O) and structural defects induce that deep levels form into the band gap. As a consequence luminescence spectra show, due to transitions to these and other deep levels, a wide band that ranges from 1.7 to 2.8 eV[4].

Isovalent impurities in II-VI compounds produce several effects on its physico-chemical characteristics [5]. In the case of Te-doped ZnO the passivation of V_O by Te atoms and changes in the atomic and energy structures due to the bigger size and lower electronegativity of Te are expected. Bigger size of Te atoms in O sites induces compression of the nearest neighbours in a first consideration. But, on the other hand, Te in O sites creates a ZnTe subunit in the ZnO lattice, and both compounds

have different lattice structures. On the other hand, Te has lower vapour pressure than oxygen, which is favourable to keep low the vacancy concentration if it occupies these sites. Lower Te electronegativity leads it acts as an isoelectronic donor, since electrons are less bound than by O atoms and a center $\{V_O^+ + D^- + Te_O^0\}^0$ forms.

Structurally, Te atoms in O sites leads the four Zn atoms nearest to Te site relax outward with relatively high displacements, the second nearest neighbour O atoms must also relax although less than Zn atoms, and third neighbours likely have negligible or none displacements as reported in substituting one S with Te[6]. Like in ZnS, Te isovalent substitution in ZnO would not form deep-level states inside the gap. However, vacancy, anti-site, and interstitial defects would do[6].

In this work, Te-doped ZnO micro and nanostructures from TeO_2 precursor by the method of sintering of compacted powder under argon flow, which leads to the growth of the structures directly on the sample surface, which acts as source as well as substrate in a vapour–solid (VS) process [4,7,8], is presented. Parts of this work were published in Superlattice and Microstructures 43 (2008) 600 and J. Mater. Sci. 43 (2008) 2844.

2 Experimental

The raw materials were commercially available ZnO powder (99.9% purity from Aldrich) and TeO_2 powder (99.9995% purity from Puratronic). TeO_2 concentration used corresponded to 0.18 at.% (sample M5), 0.92 at.% (sample M6) and 1.89 at.% (sample M7) Te. The mixed powders were milled for 10 h in a Retsch S100 centrifugal agate ball mill. Afterwards, the milled powders were compacted under a 2 T compressive load to form disc-shaped samples of about 7 mm diameter. The samples were then placed on an alumina boat near the gas inlet in a furnace, and sintered at 1270 °C under 2 litres per minute argon flow for 15 hours. The morphology and size of the structures have been investigated by scanning electron microscopy in a Leica 440. CL measurements were carried out at room temperature on the Leica 440 SEM. In order to evaluate the sample quality we use a figure of merit given by the ratio, r_I, between the main near band edge peak, I_{be}, and the defect band, I_{db}, intensities, $r_I = \frac{I_{be}}{I_{db}}$, i. e., the higher ratio the better quality. CL images were recorded by using a Hamamatsu R928 photomultiplier and CL spectra were obtained with a Hamamatsu PMA-11 CCD camera. X-ray microanalysis was performed using a JEOL JXA-8900 Superprobe by energy dispersive spectroscopy (EDS).

3 Results and discussion

3.1 Pure ZnO. As a reference, a pure ZnO sample (M0) was prepared and thermally treated. Fig. 1a shows well defined polycrystalline morphology of this undoped sample and Fig. 1b shows the CL spectra. It is formed by several contributions and the defect band is high and relevant.

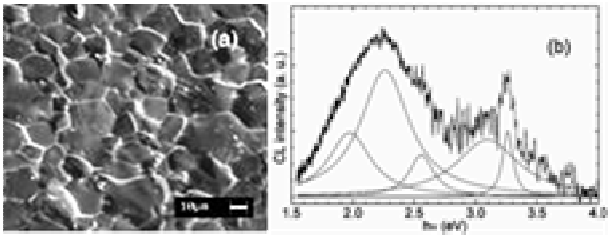

Figure 1. a) Surface morphology and b) CL spectrum of a pure ZnO sample.

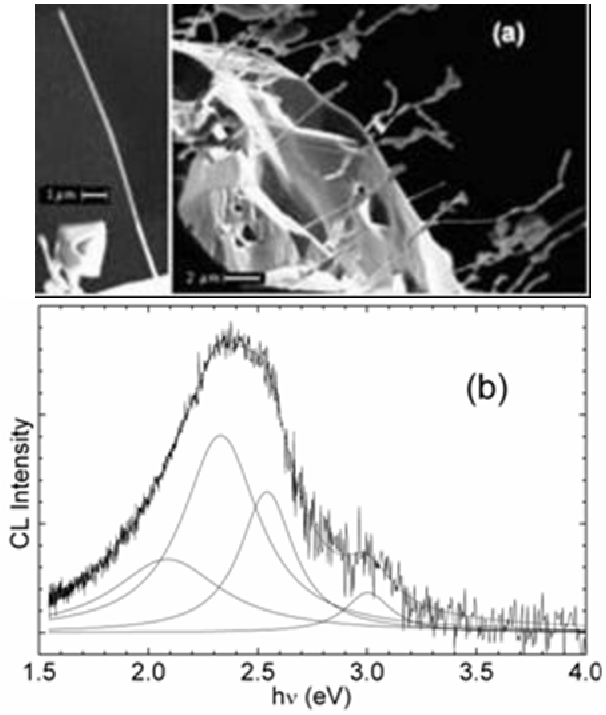

Figure 2. Image of a group of spout-like structures (a) and CL spectrum in the head of one of them (b) in sample M5.

To estimate such contributions the CL spectrum was deconvoluted with Lorentzian fitting. Five main bands at about 1.97, 2.26, 2.56, 3.10, 3.26 eV can be resolved. The band at $h\nu_{max} \approx 1.97$ eV has been associated to Zn vacancies, V_{Zn} [9] and the band centred at $h\nu_{max} \approx 2.26$ eV has been proposed as due to either singly ionized O vacancies[10] or insterstitial Zn[11]. A very wide band at $h\nu_{max} \approx 2.56$ eV, which has been observed at nearby values[12,13] has not a totally clear origin, but has been ascribed to oxygen vacancy[12]. The wide peak centred at $h\nu_{max} \approx 3.10$ eV can be related to overlapping of transitions to levels due to dislocations[13], interstitial Zn [12] and to the grain boundary, which introduces a level at 0.33 eV below the conduction band[14]. FWHM`s of these component bands are high (≥ 0.24 eV), which identifies a high statistical dispersion of the deep-level energy band distortion. The

ZnO band edge emission is centred at $h\nu_{max} \approx 3.26$ eV as it has been previously reported at that position[12,15,16] and it has a typical width of FWHM ≈ 0.10 eV. Thus, the treated pure ZnO samples are very defective with high concentrations of Zn and O vacancies and intertitials, dislocations and grain boundary defects. The quality factor is as low as $r_l \approx 0.7$.

We have to point out that under the processing conditions only one kind of structures, spout-like ones, grows in milled pure ZnO samples, conversely to those found in unmilled ZnO[4]. Such structures are analysed below. Doped samples showed several micro and nanostructured shapes, which grow in the sample surfaces.

3.2 Spout-like nanostructures. Fig. 2a shows elongated spout-like nanostructures in sample M5, which grow mainly in the rim of the sample and they are typical for all the samples, even for pure ZnO samples. They have thin stems of about 100 to 300 nm diameter, which augments toward the tip with rounded polymorph forms, and the aspect ratio reaches values as high as 1:120. CL spectra in the head of these structures are practically constituted by a unique yellow-green defect band, which indicates they are highly defective as observed in Fig. 1b. Lorentzian deconvolution gives the contributions of Zn and O vacancies and interstitial Zn. The structures do not show grain formation, however, given that these nanostructures are also present in undoped ZnO samples, we associate the 3.00 eV peak with surface and dislocation effects[13].

3.3 TeO_2 doped ZnO samples. All sample surfaces look eroded and with sintered grains forming little conglomerates as can be observed in the background of Fig. 4a. CL spectra of the annealed samples over a relatively wide surface region (Fig. 3), where no structures there were, show a main intense peak in the violet region. On the high energy side a little shoulder remarks, which is a satellite band related with the ZnO emission contribution. By Lorentzian fitting two main peaks were found. A very wide peak was found at about $h\nu \approx 2.9$ eV with FWHM ≈ 0.55 eV and an intense peak at about $h\nu_{max} \approx 3.13$ eV with FWHM ≈ 0.2 eV. The CL peak energy at $h\nu_{max} \approx 3.13$ eV is lower than that of pure ZnO shown in Fig. 1b. If the ZnTeO phase forms the fundamental gap decreases from the ZnO gap energy below 3.25 eV according to the $ZnTe_xO_{1-x}$ composition[17]. The peak at $h\nu \approx 2.9$ eV was associated to grain boundaries and dislocations and its very high FWHM is consistent with the highly eroded surface. A careful Lorentzian fitting processing of the main peak allowed deconvoluting the little overlapped peak at the high energy side. This peak is at about $h\nu \approx 3.28$ eV with FWHM ≈ 0.07 eV and is associated to pure ZnO with relatively low disorder. It is noticeable that the typical ZnO green-yellow defect band is not present, which indicates a high quality ratio r_l. The absence of the defect band is related to substitutional Te in the O vacancies and passivation of the defects in the sample under treatment. On the low energy side of the main peak an exponential band tail is also observed, which is associated to structural disorder, which introduces localized levels and extends the band into the energy band gap[18]. The corresponding tail parameters range as $E_0 \approx 160 - 330$ meV, according to measured area, which are high values mainly due to structural disorder. The E_0 values are consistent with the also high FWHM of this CL peak.

XRD measurements showed that the samples have a unique ZnO phase and no TeO_2 phase was detected. Thus, we can infer that the main peak at $h\nu_{max} \approx 3.13$ eV, shifted to lower energy respect to that of ZnO, is related to the presence of ZnTe subunits, formed from the Te atoms insertion into the V_O, in the ZnO matrix, which give a pseudobinary compound $ZnTe_xO_{1-x}$. The possibility of interstitial Te was neglected since it would induce an increase of the deep level and would contribute to the defect band[6], but, conversely, the CL spectra present a clear trend to the defect band reduction with TeO_2 doping.

In order to estimate how many ZnTe subunits intervene in the $ZnTe_xO_{1-x}$ units we use a linear approximation between ZnO ($Eg_{ZnO} = 3.26$ eV) and ZnTe ($Eg_{ZnTe} = 2.26$ eV) [19,20] band gap energies given by the expression

$$Eg(x) = (1-x)Eg_{ZnO} + xEg_{ZnTe}. \qquad (1)$$

In this case band-band transitions were assumed and the shift of Eg respect to peak maximum is kT/2, where k is the Boltzman constant and T the measurement temperature.

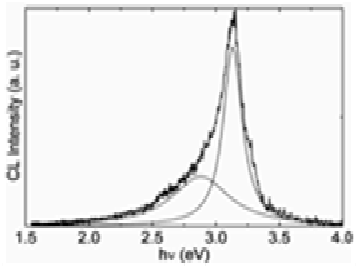

Figure 3. CL spectrum of the substrate surface after the thermal process.

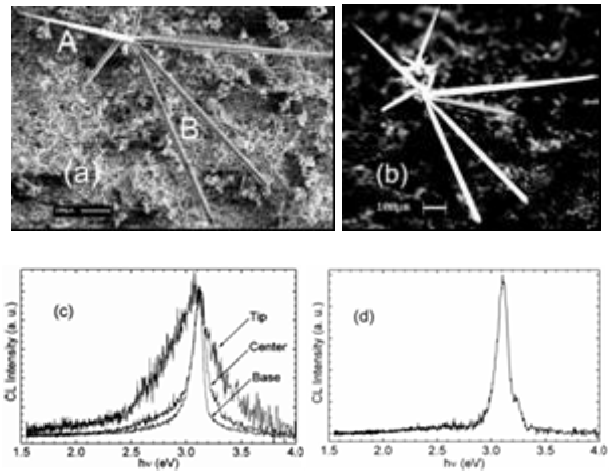

Figure 4. SEM image of a hedgehog-like structure group (a), where the needle-like structure (A) and the pencil-like structures (B) are pointed out, and CL image of this structure group (b) in the sample M5. CL spectra of needle-like (c) and pencil-like (d) structures are also shown.

3.4 Elongated microstructures. Big elongated structures grew on the sample surface. Fig. 4a shows a hedgehog-like structure group. It is formed by needle-like (A) and pencil-like (B) structures. Such structures have an aspect ratio that can reach values of 1:30 in those more developed. Fig. 4b shows CL image, where high emission of this structure group is observed.

In Fig. 4c the normalized CL spectra mapping along the needle-like (A in Fig. 4a) structure of beforementioned structure group are presented. A main feature of these spectra is that the defect band is either very small or not clearly present, however the spectra widen toward the tip and the emission intensity diminishes.

On the high energy side a shoulder can be observed. It is associated to the contribution of the pure ZnO emission. The CL emission spectra shape (Fig. 4c) show a main peak and a shoulder at the high energy region, which are associated to $ZnTe_xO_{1-x}$ and ZnO contribution respectively and no defect band is clearly appreciable. The estimation of such contributions was made by deconvoluting with Lorentzian fitting. The $ZnTe_xO_{1-x}$ peak maximum has a range $h\nu_{max} \approx 3.10 - 3.13$ eV and the ZnO peak was found at about $h\nu \sim 3.36$ eV. From Eq. 1 it was calculated that $x \approx 0.14 - 0.17$. FWHM's were of about 0.30 eV and 0.49 eV respectively. The high FWHM´s demonstrate that the coexisting $ZnTe_xO_{1-x}$ and ZnO domains are locally structurally disordered, although the absence of the defect band suggests that they are stoichiometrically ordered. Such local domains are constituted by a mixture of $ZnTe_xO_{1-x}$ with different x, i. e., a mixture of Te coordinations in the ZnO matrix, and ZnO clusters. The CL intensity was found to diminish from base to tip as the structural disorder increases, as can be correlated with the lowering of the signal/noise ratio. Analyses of the low energy side give an exponential behaviour, which corresponds to that of the band tail. The tail parameter E_0 ranges from about 100 meV in the base to 470 meV in the tip, which means that there is high structural disorder, which agrees with the previous FWHM results, and it increases from base to tip.

The structures B of Fig. 4a are partially distorted pencil-like structure, which has lost the hexagonal cross-section as reported in similar ZnO structures[4]. CL spectrum of the pencil-like structure base is displayed in Fig. 4b. The defect band is low. CL spectra along the structure show similar shapes, but the defect band lowers toward the tip. The quality ratio is high, i. e., $r_I \geq 14$. The deconvolution of the main peak using Lorentzian fitting gave that this peak is centred at a mean energy of $h\nu_{max} \approx 3.11$ eV with average FWHM ≈ 0.121 eV, which correspond to $ZnTe_xO_{1-x}$ with $x \approx 0.16$ and it overlaps a minor peak at about 3.25 eV with average FWHM ≈ 0.043 eV corresponding to pure ZnO.

In the analysis of the CL peaks it must be taken into account that pure ZnO has low CL emission. On the other hand, $ZnTe_xO_{1-x}$ has donor conductivity because of the isovalent Te doping and, therefore, it has higher carrier concentration and a higher CL intensity must be expected. Hence, although the ZnO band intensity is low, indeed, relatively high ZnO concentration can be present in comparison to $ZnTe_xO_{1-x}$ concentration. These needle-like and pencil-like structures show CL emission higher than that of the background due to the intense violet band associated with them. On the other hand, they are stoichiometrically ordered structures although some structural disorder can be found.

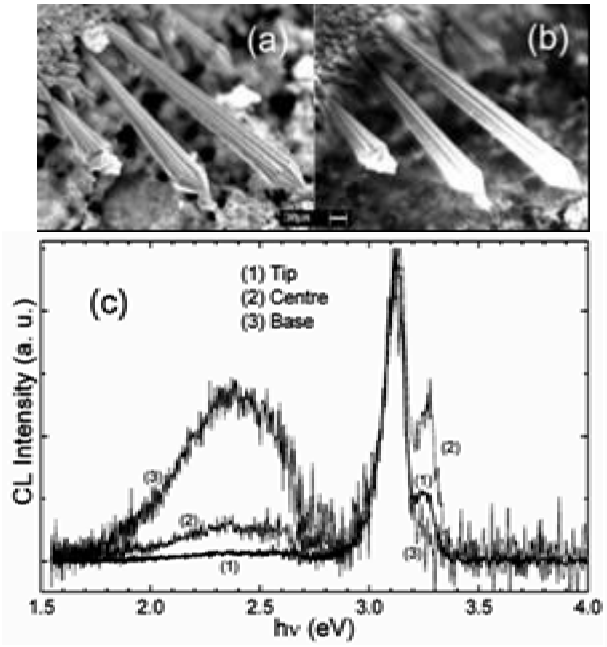

Figure 5. SEM (a) and CL (b) images of mace-like microstructures in sample M5. CL spectra (c) in several points of the biggest one are presented.

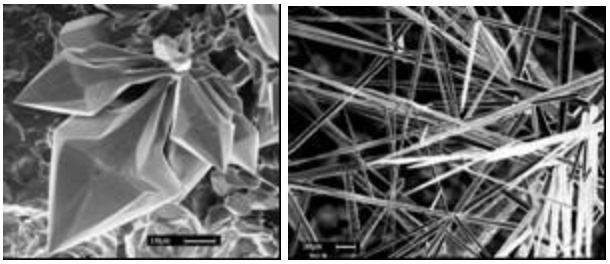

Figure 6 and 7. SEM image of arrow-like structures in sample M5 and hank structure in M6.

Other kind of structures, mace-like ones, is shown in Fig. 5a. CL emission image of the longest structures is shown in Fig. 5b. It is noticeable that the CL emission mainly takes place in the tip and diminishes toward the base. Fig. 5c shows the CL spectra along one of these structures. The quality ratio increases from about $r_I \approx 2$ at the base to about $r_I \approx 32$ in the tip where no defect band practically there is. By deconvoluting the high energy made-up peak it is found that the compound peaks corresponding to $ZnTe_xO_{1-x}$ and ZnO are at about 3.12 eV and 3.27 eV respectively. However, the FWHM tends to increases from tip to base, which corresponds to

the increase of the disorder. The increase of the defect the increase of the traps into the band gap and the decrease of the radiative emission, which explains that in the tip there is emission and in the base there is not.

The cross-section increasing from base to tip observed in Fig. 5a and the CL characteristics suggest that the structure orders as it grows. The relatively high intensity of the ZnO band in the structure centre suggests that there is high concentration of ZnO domains in comparison to $ZnTe_xO_{1-x}$, which diminished toward the tip. EDS measurement along the mace-like structures gives that the Te concentration changes from 0 at.% Te in the base and 0.02 at.% Te in the centre to 0.05 at.% in the tip. This confirms that the Te atomic concentration increases from base to tip. Thus, two favourable factors make the tip more emissive, few defects and low ZnO concentration. The CL spectrum of the little mace-like structure placed on the right of those illuminated ones is similar to that of before-showed mace-like structure base. It presents a high defect band and $r_I \approx 2$, similar to that of mace base, which suggests high defectivity and number of deep levels, which leads to low or no emission as observed in the CL image. It can be observed from comparison of CL spectra and SEM image that this structure has not developed.

Arrow-like structures as those displayed in Fig. 6 can also be observed in the region near the sample outskirts. Their base is a relatively narrow stem, but suddenly a big arrow-like head grows. CL spectra (not shown) display relatively high defective structures with $r_I \approx 4 - 6$ and FWHM $\approx$ 0.092 – 0.133 eV in the main peak, which indicates structural and stoichiometrical, disorders of the $ZnTe_xO_{1-x}$ domains.

4 Conclusions

TeO_2-doped ZnO-elongated micro and nanostructures have been grown by a vapour–solid process. The nanostructures, which arose in the sample rim, have high aspect ratio, but they seem to be defective due to vacancies. In some cases, like the elongated structures relatively far from the sample rim have low defect bands as observed in their CL spectra. This is due to Te reacts with ZnO, passivate the defects by occupying the O vacancy sites and forms $ZnTe_xO_{1-x}$ units. Other microstures, like those mace-like located in the near sample rim, have a monotonically variation of the CL intensity, due to a distribution gradient of Te along these structures. The adding of TeO_2 to the ZnO powder stimulates the growing of nano and microstuctures, however the structural, compositional and optical characteristics change according to the Te concentration and temperature gradient in each sample region.

As the TeO_2 concentration in the powder mixture increases the pure ZnO satellite band tend to decrease, and for 1.89 at.% Te only a little shoulder on the high energy side of the main peak is noticeable. The increase of the Te concentration favours the formation of a major number of structures, which form a knotty hank as exemplified in Fig. 7.

Acknowledgements

One of the authors (A.I.) would like to thank MEC España and UCM for mobility financing and facilities under SAB2005-0018. This research was partially supported by Project MAT2006-01259 and it is under PNCIT 00613457.

References

1. S. J. Pearton, D. P. Norton, K. Ip, Y.W. Heo, T. Steiner, Progress in Materials Science 50, 293 (2005).
2. S. T. Tan, B. J. Chen, X. W. Sun, W. J. Fan, H. S. Kwok, X. H. Zhang and S. J. Chua, J. Appl. Phys. 98, 013505 (2005).
3. T. Makino, K. Tamura, C. H. Chia, Y. Segawa, M. Kawasaki and A. Ohtomo, H. Koinuma, J. Appl. Phys. 92, 7157 (2002).
4. J. Grym, P. Fernández and J. Piqueras, Nanotechnology 16, 931 (2005).
5. R. Baltramiejunas, V. D. Ryzhikov, V. Gavryushin, A. Kazlauskas, G. Raciukaitis, V. I. Silin , D. Juodzbalis, and V. Stepankevicius, Journal of Luminescence 52, 71 (1992).
6. H.J. Liu, C.T. Chan, Physics Letters A 352, 531 (2006).
7. A. Urbieta, P. Fernández and J. Piqueras, Appl. Phys. Lett. 85, 5968 (2004).
8. D. Maestre, A. Cremades and J. Piqueras, J. Appl. Phys. 97, 044316 (2005).
9. J. Piqueras and E. Kubalek, Sol. Stat. Comm. 54, 745 (1985).
10. K. Vanheusden, W. L. Warren, C. H. Seager, D. R. Tallant, J. A. Voigt, B. E. Gnade, J Appl Phys 79, 7983 (1996).
11. T. Tatsumi, M. Fujita, N. Kawamoto, M. Sasajima and Y. Horikoshi, Japanese Journal of Applied Physics 43, 2602 (2004).
12. H. He, Y.Wang and Y. Zou, J. Phys. D: Appl. Phys. 36, 2972 (2003).
13. R Radoi, P Fernández, J Piqueras, M. S. Wiggins, and J. Solis, Nanotechnology 14, 794 (2003).
14. B. J. Jin, S. Im, S. Y. Lee, Thin Solid Films 366, 107 (2000).
15. H. L. Porter and J. F. Muth, J. Narayan, J. V. Foreman, and H. O. Everitt, J. Appl. Phys. 100, 123102 (2006).
16. Y Ortega, P Fernández and J Piqueras, Nanotechnology 18, 115606 (2007).
17. M. R. Özalp, G. Özen, F. Altin, V. Kalem, and M. L.Öveçoglu, Key Engeneering Materials, 264-268, 1907 (2004).
18. A. Iribarren, R. Castro-Rodríguez, F. Caballero-Briones, and J. L. Peña, Appl. Phys. Lett. 74, 2957 (1999).
19. R. Amutha, A. Subbarayan, and R. Sathyamoorthy, Cryst. Res. Technol. 41, 1174 (2006).
20. A E Rakhshani, Semicond. Sci. Technol. 19, 543 (2004).